Compensation for 3D physiological motion in robotic-assisted surgery using a predictive force controller

Michel Dominici, Philippe Poignet, Rui Cortesão, Etienne Dombre, Olivier Tempier

Compensation for 3D Physiological Motion in Robotic-Assisted Surgery Using a Predictive Force Controller. Experimental Results

Michel Dominici[1], Philippe Poignet[1], Rui Cortesão[2], Etienne Dombre[1], Oliver Tempier[1]

[1]*LIRMM-UMR CNRS, University of Montpellier II, F-34392 Montpellier cedex 5, France*
[2]*University of Coimbra, Institute of Systems and Robotics, 3030 Coimbra, Portugal*

emails:{dominici, poignet, dombre, tempier}@lirmm.fr   cortesao@isr.uc.pt

Abstract— **This paper presents a predictive force control approach to compensate for the physiological motion induced by both respiratory and heart beating motions during cardiac surgery. It focuses on the design and implementation of the control algorithm in the context of robotized minimally invasive surgery. The controller is based on a linear predictive control loop using the force information applied on the heart by the instrument. Experimental evaluation highlights the performance of the algorithm for compensating 3D physiological motion.**

I. INTRODUCTION

To perform a cardiac operation such as a Coronary Artery Bypass Graft (CABG), the main procedure is to perform a large incision (of about $20\ cm$) to access the heart and replace blood circulation and respiration by an external system (on-pump surgery). However, the use of a heart-lung machine implies more risks and a longer recovery time for the patient [1]. Minimally invasive beating-heart robotized surgery aims at minimizing the size of the incision and removing the cardiopulmonary bypass machine.

Nevertheless, during off-pump surgery, physiological motions such as respiration and heartbeat, give rise to new problems. Respiration is the most important source of disturbances. It yields large cyclic displacements of several organs, mainly in the abdomen and thorax. Heartbeat motion involves high acceleration displacements. The sum of these motions is very disturbing for the surgeon during the operation especially for surgical procedures requiring good precision (*e.g.*, needle insertion or suturing). Indeed, the gesture accuracy strongly depends on his/her ability to compensate for these motions. Manual tracking of the complex heartbeat motion cannot be achieved by a human without phase and amplitude errors [2].

A. Related Work in the Literature

As a first approach to limit disturbances due to heartbeat motion, a mechanical device, also known as stabilizer, may be used to constrain the motion of a small area on the surface by suction or pressure. Despite many improvements since the first version in the early $90's$, stabilizers still have several drawbacks. In [3] and [4], the residual cardiac motion was evaluated through experiments on pigs using commercially passive stabilizers. In both works the results show that the residual motion is too large to realise heartbeat surgery.

Moreover the suction device may damage the myocardium tissue and it is not well suited for interventions that are located behind the heart.

To efficiently circumvent theses disturbances (breathing and heartbeat motion) with lower risks and better accuracy, robotized surgery offers another alternative through the use of computer vision and/or a force control. Vision system, firstly developed for motion planning or guidance of a manipulator [5], is used to track and compensate for the physiological motion. Recently in [6], the authors developed an active piezo-actuated compliant cardiac stabilizer, called Cardiolock. The stabilizer is controlled in one dimension using a high speed vision feedback.

In a recent work presented in [7], the control algorithm fuses information from multiple sources: mechanical motion sensors that measure the heart motion and biological signals such as electrocardiogram (ECG). The control algorithm identifies the salient features of the biological signals and merges these informations to predict the feedforward reference signal. This is intended to improve the performance of the system since these signals result from physiological processes that causally precede the heart motion.

A force feedback control allows to manage the interaction forces between the tool and the environment. In [8], the authors proposed a force feedback control (based on a PI scheme) coupled with an Iterative Learning Control where the error signal is filtered with varying cut-off frequency. The algorithm supposes that the perturbation is periodic and the period is known. Since respiration is controlled by an external ventilator device, the motion induced by respiration may be considered as periodic. This hypothesis may however be too restrictive for the random and chaotic nature of cardiac motion [9]. Tests performed on an artificial moving target with a very simple periodic movement showed large errors.

In [10] two independent Active OBservers are used for force control and motion compensation. The AOB reformulates the Kalman filter based on a desired closed loop behavior (reference model) and on an extra state enclosing an equivalent disturbance referred to the system input. First AOB is reponsible for model-reference adaptive control to guarantee a desired closed loop dynamics for the force. The second AOB performs control actions to compensate physiological motions. Simulations realised, with non sinusoidal
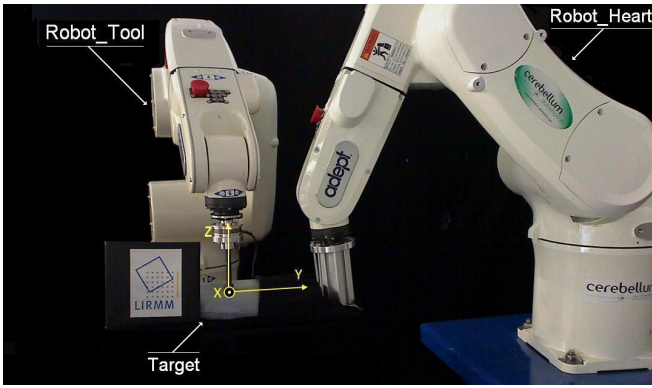
Fig. 1. Experimental platform: Robot_Tool, Robot_Heart and the target. A frame in attached at the Robot_Tool tip.
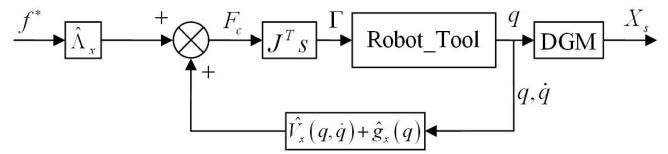

Fig. 2. Decoupled system in the Cartesian space (DGM: Direct Geometric Model)

problem is explained in the section III. The experimental results are presented in section IV. Finally, our conclusions are drawn in section V.

II. PLATFORM

A. Experimental Setup

The experimental platform is composed of two 6-DOF Viper s650 robots and a target in foam (Fig. 1). The first robot, Robot_Heart, controlled in position, is used to animate the target with real $3D$ physiological motion recorded on a pig (cardiac and respiration motions). The second one, Robot_Tool controlled in force, holds the surgical instrument and applies a force on the moving target. An ATI Mini-45 force sensor is attached to its end-effector to measure the applied force. An ATI Nano-17, attached to the tool, may be used for minimally invasive surgery. The controllers are implemented on a $2.4\ GHz$ Intel Core Duo processor running on Windows XP and communicate with the robots via a MotionBlox-60R from Adept and a FireWire connection. The MotionBlox-60R verifies the integrity of the robots using protections such as *Watchdog* functions, testing maximal velocity, joint position limits and tracking errors. The closed loop sampling time of the controller is $T_s = 1\ ms$ and $125\ \mu s$ for the protection functions.

disturbance force, highlights good performances of the approach.

B. Motivation and Methodology

In minimally invasive cardiac surgery, the workspace available during the operation is limited. Therefore, heart motion compensation should be performed with instruments already available in conventional minimally invasive surgeries, thus discarding the use of additional markers or sensors placed on the heart surface.

Using, for instance, only vision systems may present two major drawbacks. First, the operation is performed in a cluttered environment. The instruments must remain in the visual field of view of the camera, often occluding the region of interest. This results in a deterioration of the tracking efficiency and consequently disturbs the overall motion compensation. A possible solution is the introduction of additional sources of information such as electrocardiogram signal, in addition to the visual feedback. Second, the visual motion compensation does not take into account the effect of the gesture performed by the surgeon on the heart surface. Contact tasks deform the surface of soft tissues locally which may modify dramatically the natural heart motion. Moreover, during a contact task, physiological motions induce disturbance forces that can hardly be appreciated and compensated with vision data.

During free heart beating, individual points on the heart move in the range of 7-10 mm. Although the dominant mode of the heart motion is in the order of 1-2 Hz, the measured motion of individual points on the heart during normal beating yields significant energy up to frequencies of 20 Hz [11]. In our approach, we consider simultaneously the two main sources of physiological motion, breathing movement and heartbeat, as disturbances. Extending the approach proposed in [12] to compensate for perturbations along one dimension, the results presented in this paper are based on a predictive controller using the measured force applied on the heart by the instrument along the three directions. Section II describes then the experimental platform and the modeling of the global system. Control algorithm used for the compensation

B. Modeling

The dynamic model of the robot holding the tool (Robot_Tool) is given by

$$\mathbf{M}\ddot{\mathbf{q}} + \mathbf{v}(\mathbf{q}, \dot{\mathbf{q}}) + \mathbf{g}(\mathbf{q}) = \tau \qquad (1)$$

where $\mathbf{q}$, $\dot{\mathbf{q}}$ and $\ddot{\mathbf{q}}$ are the vectors of respectively joint positions, velocities and accelerations; $\mathbf{M}$ is the mass matrice; $\mathbf{v}(\mathbf{q}, \dot{\mathbf{q}})$ is the vector of Coriolis and centrifugal torques; $\mathbf{g}(\mathbf{q})$ is the vector of gravity torque and τ is the generalized torque acting on the joints.

Using the operational space formulation, (1) can be written as

$$\mathbf{\Lambda}_x \ddot{X}_s + \mathbf{V}_x(\mathbf{q}, \dot{\mathbf{q}}) + \mathbf{g}_x(\mathbf{q}) = F_c \qquad (2)$$

where $\mathbf{\Lambda}_x$, $\mathbf{V}_x(\mathbf{q}, \dot{\mathbf{q}})$ and $\mathbf{g}_x(\mathbf{q})$ are respectively the mass matrix, the Coriolis and centrifugal torque vector and the gravity torque vector written in Cartesian coordinates [13], [14]; F_c denotes the commanded force. Further details including numerical data useful for the implementation may be found in [15].

Assuming[1]

$$\hat{\mathbf{\Lambda}}_x = \mathbf{\Lambda}_x \quad \hat{\mathbf{V}}_x = \mathbf{V}_x \quad \hat{\mathbf{g}}_x = \mathbf{g}_x \qquad (3)$$

[1]The expression of form "$\widehat{A}$" means "an estimation of the variable A"
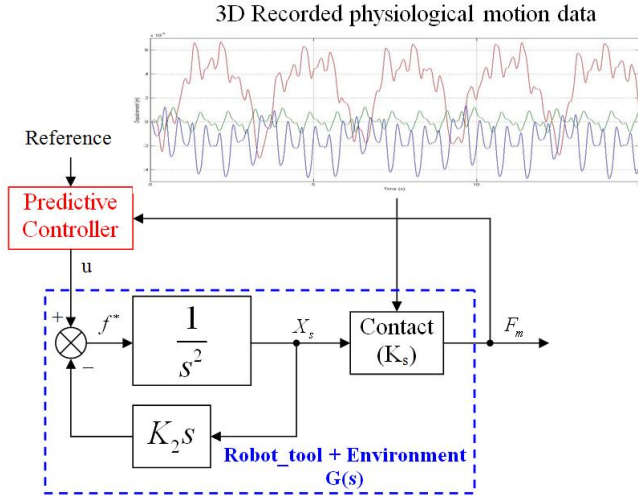
Fig. 3. Global control scheme with the linear predictive force controller, the linearized Robot_Tool and the model of the contact (environment) animated by recorded $3D$ physiological motion data.

and choosing

$$F_c = \hat{\mathbf{V}}_x(\mathbf{q}, \dot{\mathbf{q}}) + \hat{\mathbf{g}}_x(\mathbf{q}) + \hat{\mathbf{\Lambda}}_x f^\star \qquad (4)$$

we obtain

$$\ddot{X}_s = f^\star \qquad (5)$$

Equation (5) represents the dynamics of a unitary mass. $f^\star$ is homogeneous to an acceleration. The decoupled system in the Cartesian space is shown in Fig. 2.

Introducing K_2 (damping loop) and a basic contact model[2] represented by K_s (environment stiffness), the global model represented in Fig. 3 becomes

$$\frac{F_m}{u} = G(s) = \frac{K_s}{s(s + K_2)} \qquad (6)$$

The transfer function $G(s)$ represents the decoupled system Robot_Tool and the model of the contact (a simple stiffness K_s) animated with recorded physiological motion data acting as a disturbance. u is the command calculated by the predictive force controller whose inputs are the reference which may be the desired surgeon force obtain through an haptic interface and F_m, the forces applied by the instrument (tip of the Robot_Tool) on the target.

The equivalent representation of $G(s)$ in time domain is given by

$$\ddot{y}(t) + K_2\dot{y}(t) = K_s u(t) \qquad (7)$$

where $y(t)$ is the plant output (Cartesian torque at the tip of the instrument), and u is the plant input (torque).

[2]A model more complex, taking into consideration the viscoelactic and anisotropic behavior of the myocardial tissue, may be used. For our experimentations the target used a spring modelise.

III. LINEAR PREDICTIVE CONTROLLER

A. Model Predictive Control Strategy

The methodology of the Model Predictive Control (MPC) is characterized by the following strategy (Fig. 4):

- the future outputs for a determined horizon N, called the prediction horizon, are predicted at each instant t using the process model. These predicted outputs $\hat{y}(t + k|t)$[3], for $k = 1 \ldots N$, depend on the known values at the instant t (past inputs and outputs) and on the future control signals $u(t + k|t)$, $k \in [0 \ldots N - 1]$, which will be sent to the system and then calculated.
- the reference trajectory $w(t + k|t)$ defines an ideal trajectory that the plant output should follow to reach the setpoint. Starting at the current output, it defines the dynamic behaviour of the controlled plant.
- the set of future control signals is calculated by optimizing a determined criterion to keep the process as close as possible to the reference trajectory. This criterion takes the form of a quadratic function of the errors between the predicted output signal and the reference trajectory. The control effort is included in the objective function. An explicit solution may be calculated if the model is linear.
- only the first element of the calculated control sequence $u(t|t)$ is sent to the process. The horizon is translated in the future and the algorithm is repeated with updated values.
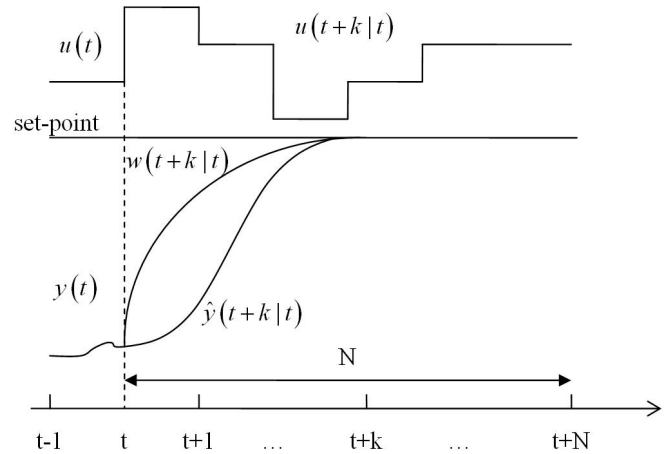

Fig. 4. MPC strategy

B. Formulation of MPC

The internal model, $G(s)$ (6), is used to predict the future plant output. It is based on the past and current states of the system and on the proposed optimal future control actions. This model includes the Robot_Tool and the environment.

[3]The notation indicates the value of the variable at the instant $t + k$ computed from intant t

Defining the state variables $x_1(t) = y(t)$ and $x_2(t) = \dot{y}(t)$, (7) can be written as

$$\begin{bmatrix} \dot{x}_1(t) \\ \dot{x}_2(t) \end{bmatrix} = \begin{bmatrix} 0 & 1 \\ 0 & -K_2 \end{bmatrix} \begin{bmatrix} x_1(t) \\ x_2(t) \end{bmatrix} + \begin{bmatrix} 0 \\ \hat{K}_s \end{bmatrix} \quad (8)$$

where $\hat{K}_s$ represents an estimation of the contact stiffness.

Discretizing (8) with sampling time T_s, the equivalent discrete time system is:

$$\begin{cases} x(k+1) = \mathbf{A}x(k) + \mathbf{B}u(k) \\ y(k) \quad = \mathbf{C}x(k) \end{cases} \quad (9)$$

The predictions along the horizon are given by

$$\hat{y} = \mathbf{\Psi}x(k) + \mathbf{\Upsilon}u(k-1) + \mathbf{\Theta}u \quad (10)$$

with

$$\mathbf{\Psi} = \begin{bmatrix} \mathbf{CA} \\ \mathbf{CA}^2 \\ \cdots \\ \mathbf{CA}^N \end{bmatrix} \quad \mathbf{\Upsilon} = \begin{bmatrix} \mathbf{CB} \\ \vdots \\ \displaystyle\sum_{i=0}^{N-1} \mathbf{CA}^i\mathbf{B} \end{bmatrix}$$

$$\mathbf{\Theta} = \begin{bmatrix} \mathbf{B} & \cdots & 0 \\ \mathbf{C(AB+B)} & \cdots & 0 \\ \vdots & \ddots & \vdots \\ \displaystyle\sum_{i=0}^{N-1} \mathbf{CA}^i\mathbf{B} & \cdots & \mathbf{B} \end{bmatrix} \quad (11)$$

The prediction (10) is composed of three terms: the first two depend on the past and current states and are known at instant k. They represent the *free response* of the plant. The third term depends on the vector of future control actions and is the key variable to be calculated. $\mathbf{\Theta}$ represents the response of the model to a unit step input.

The control sequence $\mathbf{u}$ is calculated by minimizing the objective function

$$J = \delta(\mathbf{\Theta}u + \mathbf{\Psi}\hat{x}(k) - \mathbf{w})^T(\mathbf{\Theta}u + \mathbf{\Psi}\hat{x}(k) - \mathbf{w}) + \lambda \mathbf{u}^T\mathbf{u} \quad (12)$$

Thus the analytical solution is given by

$$\mathbf{u} = (\delta\mathbf{\Theta}^T\mathbf{\Theta} + \lambda I)^{-1}\delta\mathbf{\Theta}^T(\mathbf{w} - \mathbf{\Psi}\hat{x}(k) - \mathbf{\Upsilon}u(k-1)) \quad (13)$$

where δ and λ are respectively the error and effort control weights.

The reference trajectory $\mathbf{w}$ approaches the set-point exponentially from the current output value. The "time constant" T_{ref} of the exponential defines the speed of the response. If the current error between setpoint $s(k)$ and output plan $y(k)$ is:

$$\epsilon(k) = s(k) - y(k) \quad (14)$$

then the reference trajectory is chosen such that the error i steps later would be:

$$\epsilon(k+i) = \lambda^i\epsilon(k) \quad (15)$$

where

$$\lambda = e^{-T_s/T_{ref}} \quad (16)$$

The reference trajectory is defined by:

$$w(k+i|k) = s(k+i) - \lambda^i\epsilon(k) \quad (17)$$

with $0 < \lambda < 1$.

Since receding horizon strategy is used, only the first element of the control sequence is sent to the plant and then all the computation is repeated in the next sampling time.
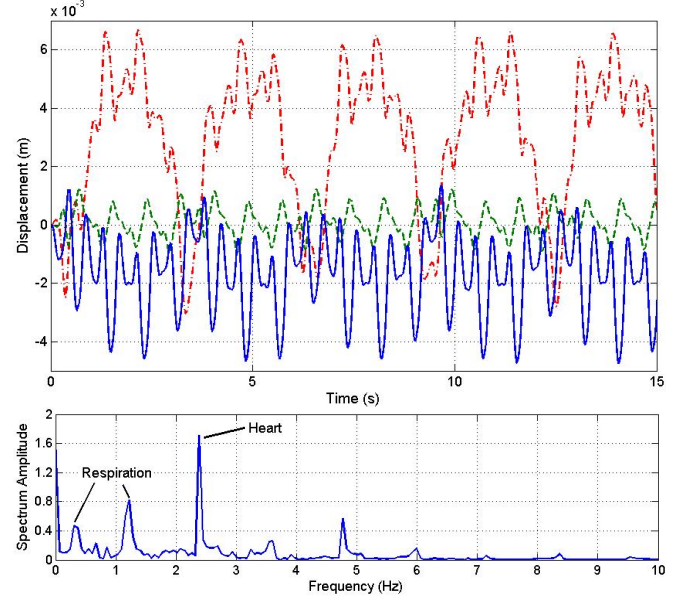

Fig. 5. Recorded physiological motion data (top). blue (solid line): X-axis, green (dashed line): Y-axis and red (dash-dot line): Z-axis. FFT spectrum of the X-axis motion (bottom). The main peaks related to the respiratory and cardiac motions are highlighted.

IV. EXPERIMENTAL RESULTS

Experimentations have been performed in order to evaluate the performance, along the three axes, of the compensation algorithm with the Force Predictive Controller presented in the previous section. The motion data used to move the target in three dimensions are shown in Fig. 5. These signals, representing the cardiac and breathing motions in $3D$, are recorded on a pig and last $15\ s$. A frequential analysis of these physiological motion data has been performed and futher details can be found in [12].

A. Predictive Controller Tuning

Four parameters are used to tune the predictive controller: the horizon value N, the "time constant" T_{ref} and the weight parameters δ and λ.

Even though tuned intuitively, we may give some guideline for tunning the horizon that may influence greatly the performance. Indeed a longer horizon results in more accuracy of the tracking reference trajectory while the calculation time of the control sequence is increased. Therefore, a horizon must be chosen so that the control sequence can be calculated within one cycle of the control loop. For the experimentations presented below, a good trade-off appears to be a constant horizon value of $N = 8 * T_s$.
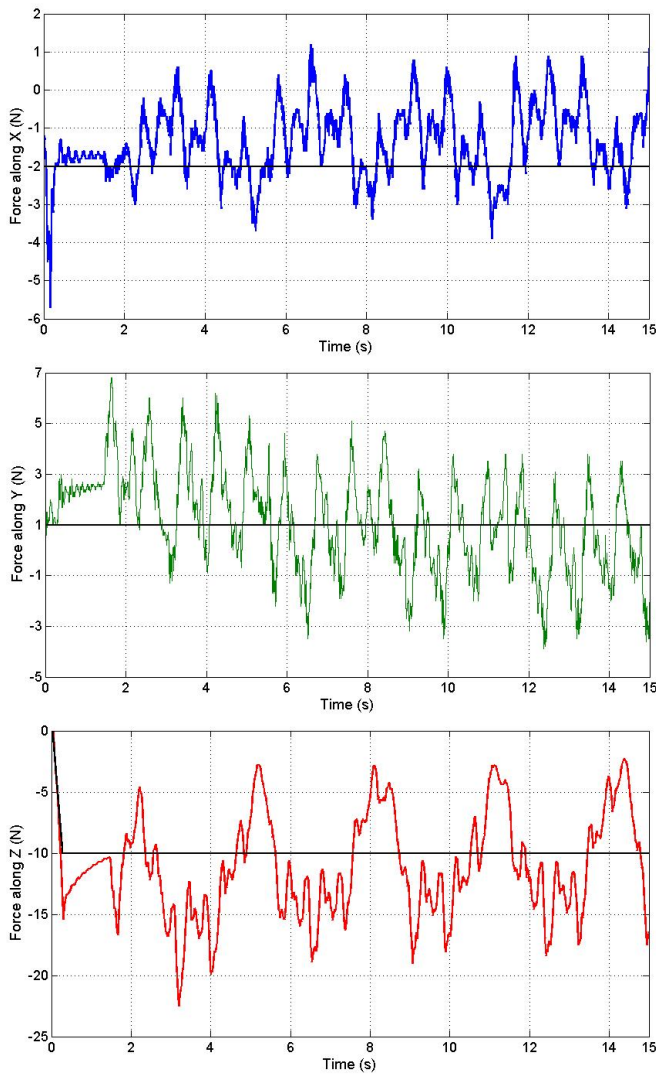
Fig. 6. No compensation - Forces applied (along X, Y and Z directions) on an moving target for a fixed desired force (-2 N for X-axis, 1 N for Y-axis and -10 N for Z-axis)

Fig. 7. With compensation - Forces applied (along X, Y and Z directions) on a moving target, for a fixed desired force (-2 N for X-axis, 1 N for Y-axis and -10 N for Z-axis)

Through the exponential "time constant" T_{ref}, the reference trajectory defines the speed of the plant response. If T_{ref} is decreased, the reference trajectory tends to a step (a large T_{ref} does not allow the system to reach the set-point). For the trajectory, to reach the set-point over the prediction horizon N, the value λ^i (16) must be close to 0 while $i = N$.

The weight parameters δ and λ are used to modify the accuracy and the control effort respectively. An increase in δ implies an increase of both accuracy and control effort. More time is consequently needed to stabilize the robot nearby the reference trajectory. Futher details for tuning parameters can be found in [12].

B. Physiological Motion Compensation

Figs. 6 and 7 represent the forces applied in the three directions by the Robot_Tool on the environment with and without compensation. The target is moving in $3D$ with the Robot_Heart following the physiological motion shown in
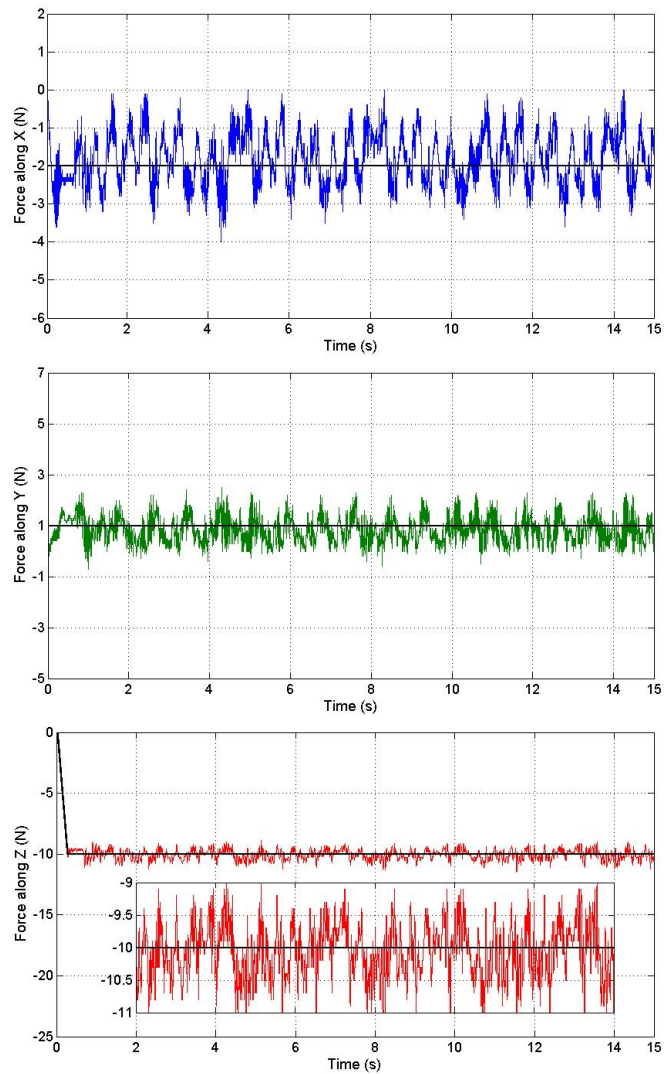
Fig. 5. The desired force is set to -2 N for X-axis, 1 N for Y-axis and -10 N for Z-axis.

Without compensation, the peak to peak error is more than 7 N on X-axis, 10 N on Y-axis and 20 N on Z-axis and the RMS error is 1 N, 1.6 N and 3.5 N along X, Y and Z axis respectively.

With compensation the maximal and RMS errors are less than 2 N and 0.5 N respectively along X-axis, 1.5 N and 0.4 N respectively along Y-axis and 1 N and 0.3 N respectively along Z-axis.

C. Discussion

Considering the two main sources of physiological motion as disturbances, compensation was achieved simultaneously along the three axes. Compared to the non-compensated case (Fig. 6), the maximal and RMS errors are decreased by 50 $\%$ for X-axis, 75 $\%$ for Y-axis and 95 $\%$ for Z-axis (Fig. 7). Even if the result on the Z-axis shows a good rejection of

the disturbance, the errors on the other axis are still too large for cardiac surgery.

We also expect to improve the performance of the controller in two ways. Firstly by improving the quality of the Robot_Tool dynamic parameters identification. These parameters, determined experimentally, are used to decouple and linearize the system (by the computed torque formulation presented in section II-B). Identification uncertainties may introduce axes coupling and/or non-linearities in the system. Therefore improving the quality of the identification should consequently improve the decoupling. Secondly replacing the ATI Mini-45 force sensor (resolution: $0.2\ N$), by an ATI Nano-17 will increase the sensor resolution ($3\ mN$) and therefore the force measure precision.

V. CONCLUSIONS

This paper has presented experimental validations of the predictive force control to compensate for physiological motion. Taking into consideration the breathing and heart beat motion along the three axes, the experimental results along Z-axis prove the efficency of the force feedback for the compensation problem.

Dynamic parameters more precise and an upgrade of the force sensor will improve the global performance of the system.

In future work, the predictive force controller will be included in the global teleoperation scheme used in [16].

REFERENCES

[1] M. F. Newman, J. L. Kirchner, B. Phillips-Bute, V. Gaver, H. Grocott, and R. H. Jones, "Longitudinal assessment of neurocognitive function after coronary-artery bypass surgery," *The New England Journal of Medicine*, vol. 344, no. 6, pp. 395–402, February 1991.

[2] V. Falk, "Manual control and tracking-a human factor analysis relevant for beating heart surgery," *The Annals of Thoracic Surgery*, vol. 74, pp. 624–628, 2002.

[3] P. Cattin, H. Dave, J. Grünenfelder, G. Szekely, M. Turina, and G. Zünd, "Trajectory of coronary motion and its significance in robotic motion cancellation," *European Journal of Cardio-Thoracic Surgery*, vol. 25, no. 5, pp. 786 – 790, 2004.

[4] M. Lemma, A. Mangini, A. Redaelli, and F. Acocella, "Do cardiac stabilizers really stabilize? experimental quantitative analysis of mechanical stabilization," *Interactive CardioVascular and Thoracic Surgery*, vol. 4, pp. 222–226, June 2005.

[5] S. Hutchinson, G. Hager, and P. Corke, "A tutorial on visual servo control," *IEEE Transactions on Robotics and Automation*, vol. 12, pp. 651–670, 1996.

[6] W. Bachta, P. Renaud, E. Laroche, A. Forgione, and J. Gangloff, "Design and control of a new active cardiac stabilizer," in *Proc. of the IEEE Int. Conf. on Intelligent Robots and Systems (IROS)*, San Diego, California, USA, 2007.

[7] O. Bebek and M. C. Çavuşoğlu, "Intelligent control algorithms for robotic assisted beating heart surgery," *IEEE Transactions on Robotics*, vol. 23, pp. 468–480, June 2007.

[8] B. Cagneau, N. Zemiti, D. Bellot, and G. Morel, "Physiological motion compensation in robotized surgery using force feedback control," in *Proc. of the IEEE Int. Conf. on Robotics and Automation (ICRA)*, Roma, Italy, April 2007, pp. 1881–1886.

[9] Y. Nakamura, K. Kishi, and H. Kawakami, "Heatbeat synchronization for robotic cardiac surgery," in *Proc. of the IEEE Int. Conf. on Robotics and Automation (ICRA)*, vol. 2, Seoul, Korea, May 2001, pp. 2014–2019.

[10] R. Cortesão and P. Poignet, "Motion compensation for robotic-assisted surgery with force feedback," in *Proc. of the IEEE Int. Conf. on Robotics and Automation (ICRA)*, Kobe, Japan, May 2009.

[11] M. C. Çavuşoğlu, J. Rotella, W. S. Newman, S. Choi, J. Ustin, and S. S. Sastry, "Control algorithms for active relative motion cancelling for robotic assisted off-pump coronary artery bypass graft surgery," in *Proc. of the Int. Conf. on Advanced Robotics (ICAR)*, Seattle, Washington, USA, July 2005, pp. 431–436.

[12] M. Dominici, P. Poignet, and E. Dombre, "Compensation of physiological motion using linear predictive force control," in *Proc. of the IEEE Int. Conf. on Intelligent Robots and Systems (IROS)*, Nice, France, September 2008.

[13] R. Cortesão, W. Zarrad, P. Poignet, O. Company, and E. Dombre, "Haptic control design for robotic-assisted minimally invasive surgery," in *Proc. of the IEEE Int. Conf. on Intelligent Robots and Systems (IROS)*, Beijing, China, October 2006, pp. 454–459.

[14] W. Khalil and E. Dombre, *Modeling, Identification and Control of Robots*, 3rd ed. Hermes Science Publications, 2002.

[15] M. Michelin, P. Poignet, and E. Dombre, "Dynamic task posture decoupling for minimally invasive surgery motions," in *The Int. Symposium on Experimental Robotics*, vol. 4, Singapore, June 2004, pp. 3625–3630.

[16] W. Zarrad, P. Poignet, R. Cortesão, and O. Company, "Towards teleoperated needle insertion with haptic feedback controller," in *Proc. of the IEEE Int. Conf. on Intelligent Robots and Systems (IROS)*, San Diego, California, USA, November 2007.